Decay of quasibounded classical Hamiltonian systems and their internal dynamics

A. J. Fendrik, A. M. F. Rivas, and M. J. Sánchez
Departamento de Física, Facultad de Ciencias Exactas y Naturales,
Universidad de Buenos Aires, Ciudad Universitaria, 1428, Buenos Aires, Argentina
(Received 15 January 1993; revised manuscript received 6 April 1994)

We study numerically the decay of a Hamiltonian system, whose transient bounded dynamics is fully chaotic but non-necessarily fully hyperbolic. We show that the fully hyperbolic character of the trapped orbits is related to a purely exponential decay law, while the existence of parabolic trapped orbits leads to a crossover between an exponential decay and an algebraic decay. We relate the behavior of the decay law to internal distributions that characterize the internal dynamics of the system.

PACS number(s): 05.45.+b

I. INTRODUCTION

The present work is devoted to studying the decay of quasibounded classical Hamiltonian systems. A quasibounded system is a system whose dynamics can be transiently bounded to a finite region of the phase space where an infinite set of nonstable periodic orbits are included before showing unbounded dynamics. The decay process is the transition from the bounded motion to the unbounded one. The decay law corresponding to a given system is related to the bounded transient dynamics. In recent works [1–3] the correspondence between the exponential decay and foregoing chaotic motion on the one hand and the algebraic decay and previous regular motion on the other hand has been extensively discussed. As it is shown in Ref. [3] through an example, this correspondence is not one to one. In other words, there are fully chaotic systems, without regular islands, whose decay law can be nonexponential. As we will show in the present work, the exponential decay is related to the fully hyperbolic subset of the invariant trapped set, that is, the hyperbolic and isolated trapped periodic orbits, while the fully chaotic systems can have nonhyperbolic (namely, parabolic orbits [4]) and nonisolated trapped periodic orbits that give rise to algebraic decay.

The invariant set of the system that we will study can be fully hyperbolic or it can have a parabolic subset according to the value of a simple parameter. Thus the decay law may be fully exponential or show a crossover between a stretched exponential and an algebraic decay. We will show how the decay law can be related to the foregoing internal dynamics.

Our work is organized in the following way. In Sec. II we introduce the system; it is geometrically similar to the Sinai billiard [5] but it is a finite well so we will call it the Sinai well. In Sec. III we show the results of a numerical study of the decay varying the control parameter that induces the mentioned behavior. Section IV shows, using ergodic properties, how the temporal decay law can be related to internal distributions that depend on the internal dynamics. In Sec. V we use the results of Sec. IV to establish the decay laws for several internal distributions. In Sec. VI we find the actual decay law to explain the results shown in Sec. III. Finally, Sec. VII is devoted to discussions and conclusions. We include three appendixes. Appendix A explores the condition having bounded motion in a finite well even with $E > 0$. Appendix B shows properties and relations among internal distributions while Appendix C shows the expected properties of the parabolic invariant subset studying Poincaré surfaces.

II. THE SINAI WELL

Let us consider a point particle of unity mass moving inside a two-dimensional square well of depth $-V_0$ ($V_0 > 0$) and side a. We distinguish three cases according to the value of the total energy $E = p^2/2 - V_0$.

(a) $E < 0$. The particle remains trapped bouncing elastically on the walls and the problem is indistinguishable from the square rigid box, i.e., a real billiard. We will call this motion billiard.

(b) $0 \leq E \leq V_0$. The particle remains in billiard motion if

$$\frac{|p_i|}{p} > \sin\psi_{\lim}\,, \tag{2.1}$$

where $i = x, y$ are the two Cartesian components of $\vec{p}$ and

$$\psi_{\lim} = \arcsin\frac{1}{\sqrt{1+V_0/E}} \tag{2.2}$$

is the limit angle. Requirement (2.1) is the condition to have an internal reflection when the particle reaches the square boundary. When condition (2.1) is not fulfilled, the particle leaves the well at most in two bounces and we will say that the particle is in free motion. For a derivation of these results see Appendix A.

(c) $E > V_0$. The particle is in free motion always.

We will restrict ourselves to case (b).

Since $|\ p_i\ |$ are constants of motion when the particle is in the billiard motion, we can distinguish two disjoint regions on the phase space: a bounded region that corresponds to the billiard motion (billiard region) and an unbounded region (free region).

As we can see, $E > 0$ is a necessary but not a sufficient condition to have unbounded motion. The accessory condition $|\ p_i\ | = \text{const}$ implies a rigid and immutable distribution of energy among the two degrees of freedom so that

$$p_x^2/2 < V_0\ , \qquad p_y^2/2 < V_0\ , \tag{2.3}$$

while $(p_x^2 + p_y^2)/2 > V_0$ and the motion remains trapped even if $E > 0$ (see Appendix A).

Now, let us place a circular obstacle, that is, a rigid circular barrier of radius $R < a/2$, in the center of the well. This change removes the condition $|\ p_i\ | = \text{const}$. In other words, the fulfillment of condition (2.1), that determines the stay of the particle inside the well, can be modified after each collision with the circular scatterer. When the particle hits the circular scatterer there is a rearrangement of the energy among the degrees of freedom. Therefore the particle could make a transition from the billiard region to the free one after colliding with the circular barrier. Our particle inside the well can be seen as a simplified model for a compound system that having enough total energy to decay it does not decay until the energy is conveniently rearranged.

In the following we will fix a (the side of the square well) as the unity of length. Moreover, accounting for the fact that $\sqrt{2(E + V_0)}$ is the modulus of the velocity because the mass m is one, the ratio $a/\sqrt{2(E + V_0)}$ has units of time, so we can take it as unity of time such that the only dependence on the total energy E is through condition (2.2). This election implies $|\ \vec{p}\ | = 1$ without loss of generality.

The Poincaré surfaces at the boundary of the well are very useful because the limits between the billiard and free regions are straight lines whose positions are determined by $\sin\psi_{\rm lim}$ given by expression (2.2). As is usual for billiards [6,7] we could plot a point each time the particle hits the boundary. The ordinate would be the tangential velocity $v_t = \cos\theta$ and the abscissa would be the distance l counterclockwise measured on the boundary from some chosen point (for example, a vertex of the square) to the point corresponding to the bounce.

When the system is a real billiard ($V_0 \to \infty$ or $E < 0$) the dynamics can be described by an area preserving map of a cylinder onto itself but as V_0 is finite and $0 < E < V_0$ there will be points mapped from the billiard to the free region. These trajectories will escape towards infinity. The present system is closely related to billiard problems with holes at the boundary, that is, on the configuration space (in particular with those of [1]). In our case condition (2.1) introduces holes into the space of momenta. Figure 1 shows the space of momenta and the mentioned holes. The momentum of the particle is represented by a point on the circumference of unity radius. The collision with the central scatterer can be seen, in such space, as a map of the circumference onto itself. If a point of the circumference is mapped in such a way that the final momentum lies on a hole (that is, $|p_x|$ or $|p_y|$ smaller than $\sin\psi_{lim}$) the particle leaves the billiard region. Moreover, as the Sinai billiard problem (without holes) is fully chaotic and ergodic, we expect that for any set of initial conditions in the billiard region the Lebesgue measure of the asymptotic trapped set will be zero when holes are introduced.

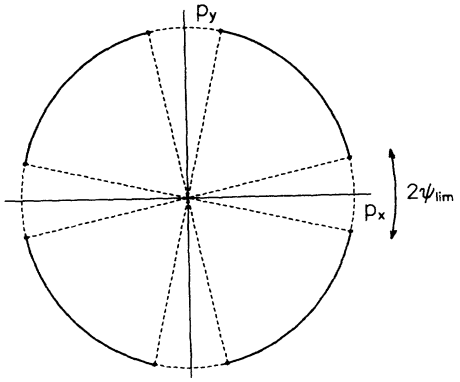

FIG. 1. Space of momenta. The momentum $\vec{p}$ lies on the circumference or radius 1. The arcs of length $2\psi_{\rm lim}$ near the axis p_x, p_y correspond to the free region (holes) while the rest of the circumference corresponds to the billiard region.

For our study we can reduce the Poincaré surface to one side by introducing appropriate variables.

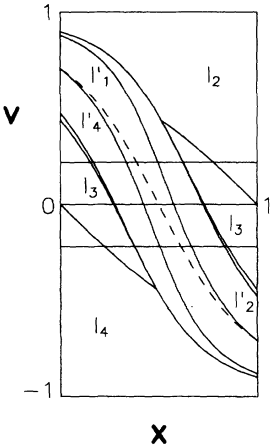

FIG. 2. Poincaré surface reduced to a side. The ordinate is v_t and the abscissa is $x = l + 1 - k$ (see the text). The horizontal straight lines show $\pm\sin\psi_{\rm lim}$ that separate billiard and free motions. The curves define regions according to which side the particle is going to. Numbering the sides in counterclockwise order, the points in I_i correspond to particles going to side $i = 1, 2, 3, 4$ missing the central scatterer. The points in the primed regions I'_i correspond to particles arriving from side i but colliding with the central scatterer. The small regions between I'_2 - I_3 and I'_4 - I_3 are I'_3.

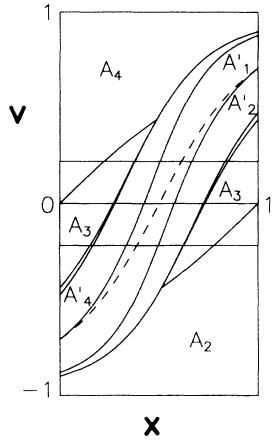

FIG. 3. Poincaré surface reduced to a side. Here the curves define regions according to which side the particles are arriving from. The points in A_i correspond to particles arriving from side i missing the central scatterer while the points in A_i' correspond to particles arriving from side i but colliding with the central scatterer. The small regions between A_2' - A_3 and A_4' - A_3 are A_3'.

$$x = (l + 1 - k) \,, \qquad v = v_t \,, \tag{2.4}$$

where $k = 1, 2, 3, 4$ numerates the sides of the square in counterclockwise order. In Fig. 2 and Fig. 3 we show such a surface. The horizontal straight lines are the limits between the billiard region ($\sin\psi_{\rm lim} < |v_t| \leq 1$) and the free region ($0 \leq |v_t| < \sin\psi_{\rm lim}$). The other curves limit the regions defined by the side of the square where the images of the points hit when they are mapped forward (Fig. 2) or backward (Fig. 3) (see Appendix C).

III. NUMERICAL STUDY OF DECAY

In this section we show the results of the numerical study of the fraction of population $N(t)/N_0$ inside the well. We start with $N_0 = 10^6$ particles whose initial conditions are random in the billiard region in all cases. Figure 4 shows $N(t)/N_0$ as a function of t for several radii ($R < 0.5$) of the circular scatterer for the fixed ratio $V_0/E = 20$. We observe two behaviors and we conclude that there is a particular radius R_c which separates them. In one case, when $R > R_c$, the decay is exponential, $\exp -\lambda t$, for all time; in the other case, when $R < R_c$, the decay is exponential for short times and it becomes algebraic, that is, $\sim 1/t^{\gamma}$ with $\gamma = 1$, for $t \to \infty$. In Fig. 5 the points show the exponents λ obtained through the best exponential fit as a function of R. For $R < R_c$ we fit only the first exponential stretch.

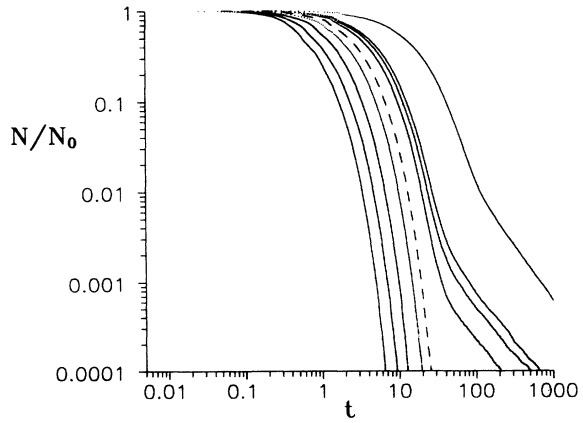

FIG. 4. Numerical results of the decay. The log-log plot shows the population N/N_0 vs t for different radii R of the central scatterer ($R = 0.499, 0.48, 0.45, 0.4, R_c, 0.3, 0.27, 0.25, 0.1$). The dashed curve corresponds to $R_c = \sqrt{2}/4$ and it separates the purely exponential decay (on the left) from the exponential decay with an algebraic long tail for long time (on the right).

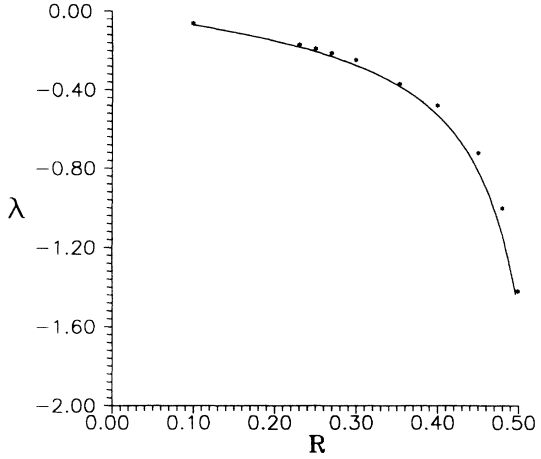

FIG. 5. Exponential decay constant λ vs R. The points correspond to the exponents obtained through the best exponential fit to the numerical results. We have considered all the decays for $R > R_c$ and only the first exponential stretch when $R < R_c$. The curve corresponds to the exponent obtained by ergodic considerations.

IV. THE DECAY

We want to relate the population $N(t)$ inside the well to the properties of the internal dynamics. We assume we have N_0 particles initially distributed according to the microcanonical distribution in the billiard region. Let $n(t) = -dN/dt$ be the number of particles that leave the well between t and $t + dt$. We can write

$$n(t) = n_1(t) + n_2(t) + n_3(t) + \cdots \,, \tag{4.1}$$

where $n_i(t)$ is the number of particles that leave the well between t and $t + dt$ after i hits against the central scatterer. We define $w < 1$ as the probability that one particle transits from the billiard region to the free region after one collision with the circular center. It can be evaluated using the ergodic theory as the ratio between all orientation of the momentum in the free region and all possible orientation of the momentum. That is,

$$w = \frac{4\psi_{\rm lim}}{\pi} = \frac{1}{\pi} \times 4 \arcsin \frac{1}{\sqrt{1 + V_0/E}} \,. \tag{4.2}$$

We also define the distributions $g(t)dt$ and $f(t)dt$ as the fraction of particles whose first collision with the central scatterer occurs between t and $t+dt$ and the fraction of particles whose time between two successive collisions with the central scatterer is between t and $t+dt$, respectively. This latter is equivalent to the free path distribution because $|\vec{p}|=$ const. The above distributions are characteristics of the internal dynamics.

With our definitions, we write

$$n_1(t) = N_0 w g(t),$$

$$n_2(t) = N_0(1-w)w\int_{t^{(1)}=0}^{t} g(t^{(1)})f(t-t^{(1)})dt^{(1)},$$

$$n_3(t) = N_0(1-w)^2 w\int_{t^{(2)}=0}^{t}\int_{t^{(1)}=0}^{t^{(2)}} g(t^{(1)})f(t^{(2)}-t^{(1)})f(t-t^{(2)})dt^{(1)}dt^{(2)},$$

$$\vdots$$

$$n_i(t) = N_0(1-w)^{i-1}w\int_{t^{(i-1)}=0}^{t}\int_{t^{(i-2)}=0}^{t^{(i-1)}}\cdots\int_{t^{(1)}=0}^{t^{(2)}} g(t^{(1)})f(t^{(2)}-t^{(1)})f(t^{(3)}-t^{(2)})\cdots f(t-t^{(i-1)})\prod_{j=1}^{j=i-1} dt^j\,. \tag{4.3}$$

Taking Laplace transform and employing the notation $\mathcal{L}[n(t)]=\hat{n}(s)$ we obtain

$$\begin{aligned}\hat{n}(s) &= \hat{n}_1(s)+\hat{n}_2(s)+\hat{n}_3(s)+\cdots \\ &= N_0 w\hat{g}(s)\{1+(1-w)\hat{f}(s)+(1-w)^2[\hat{f}(s)]^2+\cdots\} \\ &= \frac{N_0 w\hat{g}(s)}{1-(1-w)\hat{f}(s)}\,. \end{aligned} \tag{4.4}$$

Defining for convenience

$$Q(t) = 1 - N(t)/N_0 \tag{4.5}$$

we have

$$\hat{Q}(s) = \frac{w\hat{g}(s)/s}{1-(1-w)\hat{f}(s)}\,. \tag{4.6}$$

Taking into account that (see Appendix B)

$$dg/dt = -g(0)f(t)\,, \tag{4.7}$$

so that

$$\hat{f}(s) = 1 - s\hat{g}(s)/g(0)\,, \tag{4.8}$$

we finally find

$$\hat{Q}(s) = \frac{w\hat{g}(s)/s}{1+(1-w)[\hat{g}(s)s/g(0)-1]}\,. \tag{4.9}$$

Then, in order to know $Q(t)$, we must be able to inverse transform (4.9).

V. TEST

To establish the relevant characteristics of the internal distribution about the decay law, we test (4.9) using four distributions $g(t)$. Three of them lead to the well known inverse transformed Laplace function $Q(t)$. The results of the present section will be useful in Sec. VI.

A. Step function

Here we assume that $g(t)$ is a step function.

$$g(t) = \frac{[u(t)-u(t-T_0)]}{T_0}\,, \tag{5.1}$$

where $u(t)$ is the Heaviside function and T_0 its width. This means a constant rate of collisions with the central scatterer for $0<t<T_0$. For $t=T_0$ all the particles will have collided.

Using (4.7), we obtain the corresponding $f(t)$:

$$f(t) = \delta(t-T_0), \tag{5.2}$$

that is, the delta function. This means a constant time T_0 between two successive collisions for all the particles. So, the mean time between collisions is T_0.

Such distributions lead to

$$\hat{Q}(s) = \left(\frac{w}{T_0 s^2}\right)\frac{\exp(T_0 s)-1}{\exp(T_0 s)-(1-w)}, \tag{5.3}$$

that is,

$$Q(t) = \frac{w}{T_0}\int_0^t (1-w)^{[t'/T_0]}dt'\,, \tag{5.4}$$

where $[t'/T_0]$ means the integer part of t'/T_0. That is, calling $n=[t/T_0]$, we have

$$Q(t) = w\sum_{j=1}^{n}(1-w)^{(j-1)}\,, \tag{5.5}$$

and finally we find

$$\begin{aligned} Q(t) &= 1-(1-w)^n \\ &\sim 1-\exp\left[\frac{\ln(1-w)}{T_0}t\right], \end{aligned} \tag{5.6}$$

and using (4.5)

$$\frac{N(t)}{N_0} = \exp\left[\frac{\ln(1-w)}{T_0}t\right] . \tag{5.7}$$

B. Exponentially decreasing ladder

Now, we suppose $g(t)$ as a series of step functions whose heights decrease geometrically.

$$g(t) = C\sum_{j=1}^{\infty} {a_0}^{j-1}\{u(t-(j-1)T_0) - u(t-jT_0)\} , \tag{5.8}$$

with $C = (1-a_0)/T_0$ and $a_0 < 1$. In the present case we obtain

$$\hat{Q}(s) = \left[\frac{w(1-a_0)}{T_0 s^2}\right]\frac{\exp(T_0 s) - 1}{\exp(T_0 s) - [1 - w(1-a_0)]} . \tag{5.9}$$

Thus, using the preceding results,

$$\frac{N(t)}{N_0} = [1 - w(1-a_0)]^n = \exp\left[\frac{\ln[1-w(1-a_0)]}{T_0}t\right] . \tag{5.10}$$

C. Exponential function

In this case we assume that $g(t)$ is an exponential function.

$$g(t) = \frac{1}{T_0}\exp(-t/T_0) . \tag{5.11}$$

Here T_0 is the mean time between collisions. Substituting in (4.9)

$$\hat{Q}(s) = \left(\frac{w}{T_0 s}\right)\frac{1}{(1 + w/T_0)} \tag{5.12}$$

this gives

$$\frac{N(t)}{N_0} = \exp(-wt/T_0) . \tag{5.13}$$

D. Power decreasing ladder

Here we suppose that $g(t)$ is a series of step functions like (5.8) but the heights of the steps decrease according to a power law.

$$g(t) = \frac{1}{T_0\zeta(\gamma)}\sum_{j=1}^{\infty}(1/j)^{\gamma}\{u(t-(j-1)T_0) - u(t-jT_0)\} . \tag{5.14}$$

Here, $\zeta(\gamma) \equiv \sum_{j=1}^{\infty} 1/j^{\gamma}$ is the Riemann function. Thus we obtain

$$\hat{Q}(s) = \left(\frac{w}{T_0\zeta(\gamma)s^2}\right)\frac{[1-\exp(-T_0 s)]\Sigma\exp(T_0 s)}{(1 + (1-w)\{[1-\exp(-T_0 s)]\Sigma\exp(T_0 s) - 1\})} , \tag{5.15}$$

where $\Sigma \equiv \sum_{j=1}^{\infty}\exp(-T_0 sj)/j^{\gamma}$. The Laplace inverse transform of (5.15) is not a simple known function, therefore we must inverse transform numerically. However, we can study its behavior at the beginning taking the limit $t \to 0$ ($s \to \infty$). For such a limit

$$\lim_{s\to\infty}\sum_{j=1}^{\infty}\frac{\exp(-T_0 sj)}{j^{\gamma}} \sim \exp(-T_0 s) , \tag{5.16}$$

therefore (5.15) becomes

$$\hat{Q}(s) \sim \left(\frac{w}{\zeta(\gamma)T_0 s^2}\right)\frac{\exp(T_0 s) - 1}{\exp(T_0 s) - (1-w)} \tag{5.17}$$

and

$$\frac{N(t)}{N_0} \sim \exp\left[\frac{\ln(1-w)}{T_0}t\right] , \tag{5.18}$$

that is, exponential decay. To see the behavior for the long t tail we take the limit $t \to \infty$ ($s \to 0$). We restrict ourselves to $\gamma = n$ integer equal to or larger than 2. At first, we replace the sum of (5.16) by the integral

$$E_n(T_0 s) = \int_1^{\infty}\frac{\exp(-T_0 sx)}{x^n}dx. \tag{5.19}$$

Then, using the identity [8]

$$E_n(z) = \frac{1}{(n-1)}[\exp(-z) - zE_{n-1}(z)] \tag{5.20}$$

and

$$\lim_{s\to 0}\sum_{j=1}^{\infty}\frac{\exp(-T_0 sj)}{j^n} = \zeta(n) \tag{5.21}$$

we obtain

$$\hat{Q}(s) \sim \frac{T_0}{\zeta(n)s}\left[\frac{1}{T_0} - s\exp(T_0 s)E_{n-1}(T_0 s)\right], \tag{5.22}$$

that means

$$\frac{N(t)}{N_0} \sim \frac{T_0^{(n-1)}}{(t+T_0)^{(n-1)}}, \tag{5.23}$$

which is a power law decay.

In summary, we conclude that distributions $g(t)$ that decrease exponentially or faster lead to exponential decay laws while an algebraic decrease of $g(t)$ corresponds to an initial exponential decay that changes into a power law decay for long times. This fact is related to the well known anomalous diffusion and the algebraic tail for the velocity autocorrelation function that take place in the periodic Lorentz gas when the horizon of the particles becomes infinite [9–11].

VI. DECAY AND NONISOLATED PARABOLIC PERIODIC ORBITS

As we have said, the velocity autocorrelation function that corresponds to the square periodic Lorentz gas shows a crossover between a stretched exponential and an algebraic decay when the diameter of the scatterers ($2R$) is smaller than the distance between their centers ($a = 1$). This behavior can be related to the particles that travel along channels defined by the directions such that $v_y/v_x = z_1/z_2$ (here z_1 and z_2 are coprime integer numbers) and they miss the scatterers. For the square array there are at least two such open channels corresponding to x direction and y direction. Using the notation of Ref. [9], we will call these channels α and β, respectively. The number of open channels increases when the radius of the scatterer decreases. Thus when $\sqrt{5}/10 < R < \sqrt{2}/4$ we have other open channels (γ) that correspond to $v_y/v_x = \pm 1$. There is an equivalence between the mentioned channels and the nonisolated parabolic periodic orbits in the system. Let us first consider the fully billiard problem. The channels α and β correspond to particles secularly rebounding between two opposite sides missing the circular scatterer. The channel γ corresponds to particles whose velocities are parallel to the diagonals of the square ($\pm\pi/4$ directions) secularly going from one side to the adjacent and since $R < \sqrt{2}/4$ they can miss the circular scatterer. Now let us consider our system with holes in the space of momenta. Condition (2.1) introduces the billiard and free regions and the periodic orbits that correspond to α and β channels lie in the free region. Therefore there are no parabolic periodic orbits trapped on the billiard region unless $R < \sqrt{2}/4$ and in such a case a crossover between the exponential and algebraic decay occurs, otherwise the decay is exponential for all t. These arguments together with the numerical study of Sec. III and the results of Secs. IV and V suggest the following ansatz for $g(t)$:

$$g(t) = C\Big([u(t) - u(t - T_0)] + \sum_{i=2}^{\infty} \alpha_i u(1 - (R/R_{c_i})) D_i(1 - (R/R_{c_i})) \times \sum_{j=2}^{\infty} (1/j)^2 \{u(t - (j-1)T_0) - u(t - jT_0)\} \Big), \tag{6.1}$$

where $D_i(x)$ are monotonic increasing functions of x between 0 and 1 such that $D_i(0) = 0$ and $D_i(1) = 1$, α_i are weight constants, and C is the normalization constant. The first contribution to (6.1) is the step function and it is responsible for the initial exponential stretch. The second, when it does not vanish (that is, at least $R < \sqrt{2}/4$), comes from particles whose positions and velocities lie close to those corresponding to parabolic orbits (open channels in the Lorentz gas). The ratios $\alpha_i u(1 - (R/R_{c_i})) D_i(1 - (R/R_{c_i}))/C$ can be seen as the fraction of the initial distribution on the phase space closest to the parabolic orbits that results when $R < R_{c_i}$.

As we have just said, we assume that the first term of (6.1), namely, the step function $[u(t) - u(t - T_0)]$ gives rise to the initial exponential stretch in the decay law. So, according to (5.7) or (5.18), T_0 must be related to the exponent

$$\lambda = \frac{\ln(1-w)}{T_0}. \tag{6.2}$$

On the other hand, the ergodic result for the mean time between collisions is known [12]:

$$\tau = \frac{(1 - \pi R^2)}{2R}. \tag{6.3}$$

When $R > R_{c_1}$, we have

$$T_0 = \tau \tag{6.4}$$

because in such a case, T_0 is the mean time between collisions. But what happens when $R < R_{c_1}$? To answer this question, Fig. 5 shows the exponent resulting from the best exponential fit to the stretch exponential decay together with the exponent predicted by (6.2) assuming $\tau = T_0$ as a function of R. The agreement between the curves suggests that

$$T_0 = \frac{(1 - \pi R^2)}{2R} \tag{6.5}$$

even when $R < R_{c_1}$. Let us remark that τ is the mean time between collisions only when $R > R_{c_1}$. If $R < R_{c_1}$, τ is the mean time between collisions for the fraction of particles that decays exponentially. That is, the ergodic result (6.3) is valid only for the hyperbolic region of the phase space.

In the following we will use (6.1) to extract information about the internal dynamics from the observed decay in Sec. III.

We restrict ourselves to the case of one open channel. In other words, there are only parabolic periodic orbits such that $v_y/v_x = \pm 1$. Because in this case there is only one critical radius, in the following we drop the subindex. That is, we rename $R_c = R_{c_1} = \sqrt{2}/4$.

Calling

$$\alpha_1 D_1(1 - (R/R_c)) = \Delta(R) \tag{6.6}$$

and using (4.9) and (6.1) we obtain

$$\hat{Q}(s) = \frac{w}{T_0\{1+\Delta(R)[\zeta(2)-1]\}s^2} \times \frac{[1-\exp(-T_0 s)]\exp(T_0 s)[\exp(-T_0 s)+\Delta(R)\Sigma']}{1+(1-w)\{[1-\exp(-T_0 s)]\exp(T_0 s)[\exp(-T_0 s)+\Delta(R)\Sigma']-1\}}, \quad (6.7)$$

where $\Sigma' \equiv \sum_{j=2}^{\infty} \exp(-T_0 s j)/j^2$ and we have used the normalization constant

$$C = \frac{1}{T_0\{1+\Delta(R)[\zeta(2)-1]\}}. \quad (6.8)$$

Δ is the only free parameter of (6.7) so inverse transforming numerically (6.7) and fitting the actual decay we have determined $\Delta(R)$ for several R. The results are shown in Fig. 6. Then assuming the simple form for $\Delta(R)$,

$$\Delta(R) = \alpha\left(1-\frac{R}{\sqrt{2}/4}\right)^{\beta}, \quad (6.9)$$

since

$$\ln\Delta = \beta\ln(1-R/R_c) + \ln\alpha, \quad (6.10)$$

β and α can be determined through the best linear fit. We have obtained $\beta = 1.4776$ and $\alpha = 0.2741$. The fit is shown in Fig. 6. Figure 7 shows the decay predicted by (6.7) using (6.9) and the above parameters for four R's that correspond to systems with only one open channel (only one parabolic region) and the corresponding actual decay calculated numerically as in Sec. III.

The parameter $\beta = 1.4776$ is consistent with the results obtained through the study of the Poincaré surface on the boundary (see Appendix C) that leads to

$$D_1 = \frac{(1-R/R_c)^2}{(1-R/2R_c)}. \quad (6.11)$$

VII. SUMMARY AND CONCLUSIONS

In the present work we have studied the decay of a transient bounded system that does not have regular islands in the phase space. We have established two well defined behaviors depending on the values of the parameter R. Both kinds of behavior are separated by a critical value $R = R_c$. One of them corresponds to a purely exponential decay law and it occurs for $R > R_c$ while the other shows a crossover between a stretched exponential and an algebraic decay ($\sim 1/t$) and it occurs when $R < R_c$. We have related this observed decay to properties of the internal dynamics using the ergodic assumption that the velocities of particles hitting the central scatterer between t and $t+dt$ are uniformly oriented after colliding. Under this hypothesis we have shown that distributions $g(t)$ such that all the particles inside the well collide with the central scatterer after a finite time (finite horizon), that is, exponentially or faster decreasing $g(t)$, lead to a purely exponential decay law. On the other hand, when $g(t)$ has any algebraic tail for long times ($1/t^{\gamma}$) the decay law shows a crossover between an exponential initial decay and an algebraic tail for long times.

In our system, finite horizon implies that only periodic orbits with at least one collision with the scatterer are allowed in the billiard region. This kind of orbit is hyperbolic due to the divergent properties of the circular obstacle. Thus the purely exponential decay corresponds to a fully hyperbolic billiard region and the invariant set of trapped conditions will be the mentioned hyperbolic

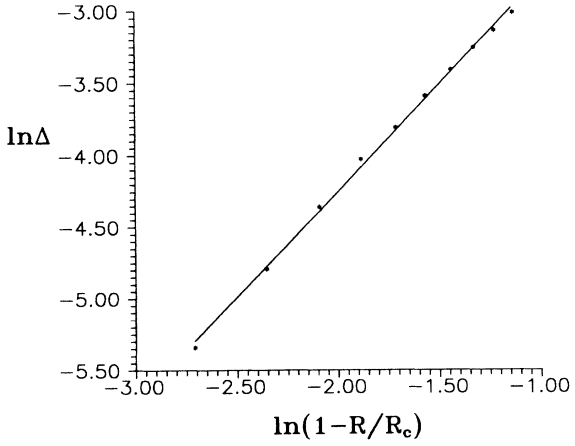

FIG. 6. The best linear fit to $\ln\Delta$ vs $\ln(1-R/R_c)$ determines $\beta = 1.4776$ and $\alpha = 0.2741$.

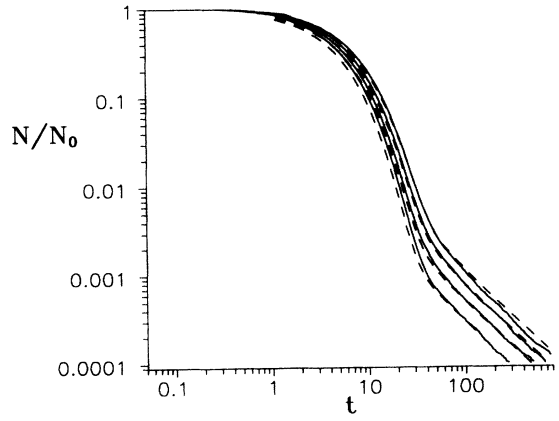

FIG. 7. Actual decay (solid lines) and predicted decay (dashed lines) by using the Laplace inverse transformed function of expression (6.7) with $\beta = 1.4776$ and $\alpha = 0.2741$ for four radii ($R = 0.23, 0.25, 0.27, 0.29$).

periodic orbits. This set has zero Lebesgue measure and a fractal dimension. It is easy to calculate this latter for the set projected on the space of momenta using the recipe found in the introduction of Ref. [3] and Eq. (5.7) applied to the circumference of unity radius.

On the other hand, a $g(t)$ with infinite horizon is compatible with periodic orbits that miss the central scatterer. They are coincident with periodic orbits of an integrable problem, namely, the square billiard. These orbits are parabolic, that is, lightly unstable but nonisolated. Thus when there are such orbits the billiard region is not fully hyperbolic and the invariant set of trapped conditions has a parabolic subset in addition to the hyperbolic one.

Thus we conclude that the $g(t)$ of the Sinai well whose central scatterer radius is R has two contributions. The first one corresponds to particles whose initial conditions lie about the hyperbolic zone of the billiard region. We model this contribution as a decreasing step function of width $T_0(R)$ given by the ergodic theory. The second one corresponds to particles whose initial conditions are asymptotic to the parabolic periodic orbits. It must vanish for $R > R_{c_i}$ and its weight increases accordingly as R decreases starting from $R = R_{c_i}$ where these special values of R correspond to the maximum radii such that the parabolic orbit i can exist. Thus we model this contribution as an algebraic decreasing ladder times a weight function that takes into account the above properties. To test our ansatz we have considered the system when there is only one class of parabolic orbits, that is, $R_{c_2} < R < R_{c_1}$. By fitting the actual decay we obtain results that are consistent with those corresponding to study the characteristics of the internal problem, namely, the billiard.

Another phenomenon that provides information about the internal dynamics through the study of asymptotic free motion is the scattering problem. Recently, a relation between the decay problem and the time delay in the scattering problem was found for nonhyperbolic Hamiltonian systems [13]. The present way to study the decay can be improved to describe the time delay distribution in the scattering problem [14]. For this it is necessary to change $g(t)$ from one that corresponds to the microcanonical population to one appropriate to describe the scattering process.

ACKNOWLEDGMENTS

We thank H. G. Solari for useful suggestions and comments and the CONICET for financial support.

APPENDIX A

The present appendix is devoted to exploring the conditions (2.1), (2.4) and the definition of $\psi_{\rm lim}$ (2.2), to have billiard motion with total energy $E > 0$.

Let us consider the two-dimensional motion of a particle in the potential defined by

$$V(x,y) = \begin{cases} -V_0 & \text{if } x \geq 0 \text{ and } y \geq 0 \\ 0 & \text{otherwise .} \end{cases}$$

Let us suppose that the particle comes from region I and arrives at $x = 0$ in point A. The momentum of the particle $\vec{p_{\rm I}}$ defines an angle ψ_i with the normal $\hat{n}$ at A as is shown in Fig. 8(a). At first, we will study the conditions required for the particle to move into region II. Of course, the total energy E must be positive but it is not enough. Moreover, the conservation of the y component p_y of the momentum must be satisfied because the external force in this direction is zero. Thus we have the following conditions:

$$E_{\rm I} = E_{\rm II} = E \,, \tag{A1}$$

that is,

$$\frac{p_{\rm I}^2}{2} - V_0 = \frac{p_{\rm II}^2}{2} = E \,, \tag{A2}$$

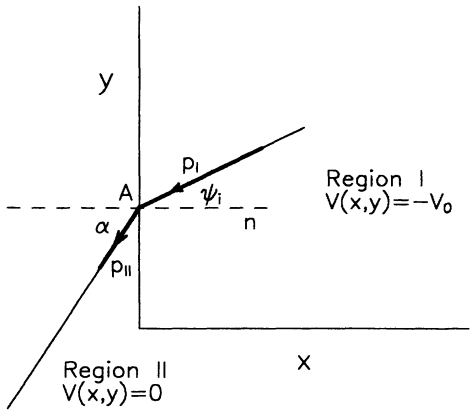

(a)

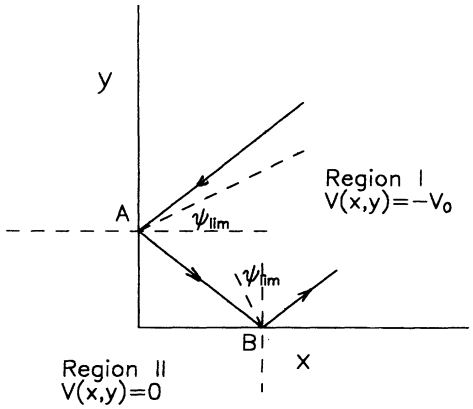

(b)

FIG. 8. One particle with total energy $E > 0$ moving on the plane x-y. In the first quadrant the potential is $V = -V_0$ (region I) while it is $V = 0$ in the others (region II). (a) The particle can enter region II because $\psi_i < \psi_{\rm lim}$ at A. (b) In this case $\psi_i > \psi_{\rm lim}$ at A and B, so the particle is reflected, remaining in region II.

and

$$p_{\mathrm{I}} \sin\psi_i = p_{\mathrm{II}} \sin\alpha \ . \tag{A3}$$

From these relations we conclude that $p_{\mathrm{II}} < p_{\mathrm{I}}$ and therefore $\psi_i < \alpha$. Because the maximum α is $\pi/2$, for a given energy there is a maximum ψ_i such that conditions (A2) and (A3) can be fullfilled. Thus, calling ψ_{lim} such an angle, from (A3), we have

$$\sin\psi_{\mathrm{lim}} = \frac{p_{\mathrm{II}}}{p_{\mathrm{I}}} \ , \tag{A4}$$

and relation (A2) implies the definition (2.2),

$$\sin\psi_{\mathrm{lim}} = \frac{1}{\sqrt{1+V_0/E}} \ . \tag{A5}$$

If $\psi_i > \psi_{\mathrm{lim}}$, that is,

$$\frac{|\,p_{\mathrm{I}_y}\,|}{p_{\mathrm{I}}} > \sin\psi_{\mathrm{lim}} \ , \tag{A6}$$

the particle is perfectly reflected and cannot enter region II.

Assuming that the particle is reflected in A, we supose it arrives at $y = 0$ in B [see Fig. 8(b)]. Now, to have a second reflection we evidently need

$$\frac{|\,p_{\mathrm{I}_x}\,|}{p_{\mathrm{I}}} > \sin\psi_{\mathrm{lim}} \ . \tag{A7}$$

Relations (A6) and (A7) are relation (2.1), that is, the condition to have billiard motion in the square well. We stress that the total energy must be $E < V_0$ because to satisfy (A6) and (A7), ψ_{lim} must be smaller than $\pi/4$.

We can develop an alternative form to formulate the conditions (2.1) using (2.2). Starting from (A6) and taking into account that $p_{\mathrm{I}} = \sqrt{2(E+V_0)}$ we get

$$p_y^2/2 > E \ . \tag{A8}$$

On the other hand, starting from (A7) we obtain

$$p_x^2/2 > E \ , \tag{A9}$$

but $E = (p_x^2 + p_y^2)/2 - V_0$ so conditions (2.3) hold.

APPENDIX B

In this appendix we discuss useful properties of distribution $g(t)$ and $f(t)$ for systems like the Sinai billiard and Lorentz gas.

Let us consider one circular scatterer of radius R immersed in a uniform bidimensional distribution of moving free point particles all of them with uniformly oriented unity velocities v. The fraction of particles that collides with the scatterer between t and $t+dt$ whose velocity subtends an angle α with the radial direction (i.e., the straight line defined by the center of the scatterer and the considered particle) is proportional to the area $I(\alpha,t)$ of a circular shell of radius

$$l(\alpha,t) = vt\cos\alpha + (R^2 - v^2t^2\sin\alpha^2)^{1/2} \ . \tag{B1}$$

That is,

$$I(\alpha,t)dt = 2\pi l(\alpha,t)\delta l(\alpha,t) \ , \tag{B2}$$

where

$$\delta l(\alpha,t) = \frac{dl}{dt}dt = \left[v\cos\alpha - \frac{(v^2\sin^2\alpha)t}{(R^2 - v^2t^2\sin^2\alpha)^{1/2}}\right]dt \ . \tag{B3}$$

To obtain $g(t)$ we must integrate (B1) over all possible α values such that the collision can occur.

$$g(t)dt \propto \left[\int_{-\alpha_1}^{\alpha_1} I(\alpha,t)d\alpha\right]dt \ . \tag{B4}$$

Here, $\alpha_1 = \arcsin[R/\sqrt{R^2+(vt)^2}]$. So, after a lengthy but straightforward calculation we obtain

$$g(t)dt \propto 4\pi vRdt \ . \tag{B5}$$

Therefore the fraction of particles that collides with the scatterer between t and $t+dt$ is independent of t. We can represent this property as a map that preserves the number of colliding particles: for each particle that collides at time t, extending its trajectory backward an arbitrary time δt, we obtain another that collides at time $t+\delta t$.

Now, let us consider a system like a Lorentz gas, that is a system of point particles as above but with many fixed scatterers. We tag a scatterer and we ask for $f(t)$, the distribution of particles whose time between a previous collision with any scatterer and the tagged one lies between t and $t+dt$. As we will see, it is closely related to $g(t)$. The above considerations show that the $g(t)$ of the actual system is modified with respect to the $g(t)$ corresponding to the system with one scatterer by the shadows and penumbras of the other scatterers. Let us consider all the particles that collide with the tagged scatterer at time t. The fraction of such particles is given by $g(t)$ and we extend their trajectories backward a time dt. There are two possibilities. (a) The prolonged trajectory lies on the sea of particles and then there is a particle that will collide at time $t+dt$ and therefore it contributes to $g(t+dt)$. (b) The prolonged trajectory penetrates into a scatterer, then it does not correspond to a colliding particle at time $t+dt$ and therefore it does not contribute to $g(t+dt)$. So we conclude that $-[g(t+dt)-g(t)]$ is proportional to the number of particles that collides with the tagged scatterer at time t after they have collided with another scatterer. Thus

$$f(t) = -\eta\frac{dg}{dt}dt \ . \tag{B6}$$

The constant $\eta = 1/g(0)$ is determined by the normalization condition

$$1 = \int_0^\infty f(t)dt = -\eta\int_0^\infty \frac{dg}{dt}dt = \eta g(0) \tag{B7}$$

because $g(\infty) = 0$.

Consequently, we obtain for the mean time between collisions τ,

$$\tau = \int_0^\infty t f(t) dt = -\frac{1}{g(0)} \int_0^\infty t \frac{dg}{dt} dt = \frac{1}{g(0)} . \tag{B8}$$

APPENDIX C

This appendix is devoted to studying the distribution $g(t)$ for long times corresponding to the billiard problem when there is a nonhyperbolic invariant subset for the decay. We will restrict ourselves to only one open channel in the billiard region, that is, to having parabolic periodic orbits such that $v_y/v_x = \pm 1$ and $\sqrt{5}/10 < R < \sqrt{2}/4$.

We will consider the dynamics on the Poincaré surface corresponding to the boundary. That is, we will study the map $(l, v_t) \to (l', v_t')$ which is induced by the dynamics on the Poincaré surface. As we have already mentioned, the symmetries of the problem (corresponding to the group C_{4v}) allow us to reduce the map to only one arbitrarily chosen side by the introduction of reduced variables

$$x = (l + 1 - k) , \qquad v = v_t , \tag{C1}$$

where $k = 1, 2, 3, 4$ numerates the sides in counterclockwise order. Figure 2 shows several curves that divide the surface in regions that are defined not only by the side where the image of each point dwells but also by the existence (or not) of an intercalated collision with the central scatterer before arriving at that side. For example, $(x, v) \in I_2$ means that the particle arrives at side 2 missing the central scatterer while $(x, v) \in I_2'$ expresses that the particle hits the scatterer before arriving at side 2. Figure 3 shows something like Fig. 2 but it is referred to the antecedent of the points (x, v). Thus $(x, v) \in A_2$ means the particle arrives from side 2 missing the central scatterer and $(x, v) \in A_2'$ corresponds to incoming particles from side 2 that have hit the obstacle before arriving. We remark that the curves of Fig. 3 can be obtained from those corresponding to Fig. 2 through the transformation $(x, v) \to (x, -v)$ which is just the time reversal transformation. We also observe that the C_{4v} symmetries are present. Thus the limiting curve that separates the regions I_2 and I_2' can be obtained from the limiting curve that separates I_4 and I_4' through the transformation $(x, v) \to (1 - x, -v)$ which corresponds to the reflection by the perpendicular plane that contains the center of the circular scatterer and the middle point of the side (that is, $x = 1/2$).

There are clockwise and counterclockwise parabolic periodic orbits. Without loss of generality we will concentrate on the former subset. Thus we are interested in studying how the intersection of the area initially defined as

$$A_4 \cap I_2 \tag{C2}$$

with its successive images decreases, that is, how the number of points arriving at side 1 from side 4 missing the circular scatterer and then going to side 2 missing the circular scatterer decreases as a function of the number of collisions with the sides, n. Figure 9 shows the initial area. The curves AB and BC are given by

$$v = \frac{(1/2 - x)\sqrt{(1/2 - x)^2 + (1/2)^2 - R^2} + R/2}{(1/2 - x)^2 + (1/2)^2} , \tag{C3}$$

$$v = \frac{(x - 1/2)\sqrt{(1/2 - x)^2 + (1/2)^2 - R^2} + R/2}{(1/2 - x)^2 + (1/2)^2} . \tag{C4}$$

They are determined by the straight lines tangent to the circular scatterer that go to side 2 or side 4 from the point x, respectively. The intersection of the parabolic invariant subset and the Poincaré surface is the segment $\overline{II'}$ where $I = (x = R/2R_c, v = \sqrt{2}/2)$ and $I' = (x = (1 - R/2R_c), v = \sqrt{2}/2)$. Here, $R_c = \sqrt{2}/4$. Therefore the length of the invariant segment is

$$L = (1 - R/R_c) . \tag{C5}$$

The map for points that go to side 2 missing the central scatterer results in

$$x' = \frac{\sqrt{1 - v^2}}{v}(1 - x) , \qquad v' = \sqrt{1 - v^2} . \tag{C6}$$

This map transforms points belonging to curve AB into points belonging to curve BC and transforms BC to curve DE of Fig. 9. Particularly we can verify that $\overline{II'}$ is transformed onto itself.

After a few iterations the area of interest is reduced to the four-sided figure shown on the right side of Fig. 10.

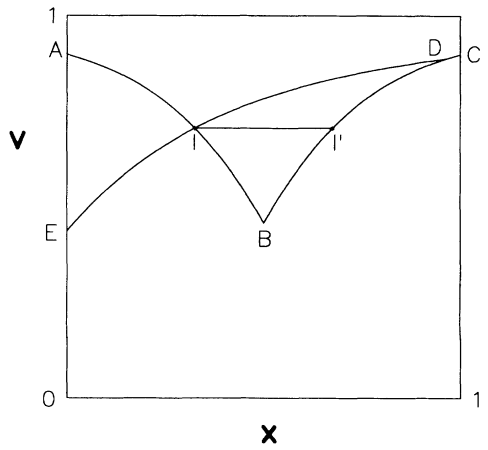

FIG. 9. Area $A_2 \cap A_4$ and the invariant subset $\overline{II'}$ corresponding to parabolic periodic orbits $v_y/v_x = \pm 1$ when $R = 0.23$.

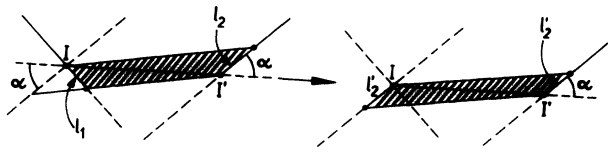

FIG. 10. Transformation of the area that remains near the invariant subset $\overline{II'}$ when $t \to \infty$.

This quadrilateral is transformed into the approximate parallelogram of equal area shown on the left. We can see that a triangular portion of such a parallelogram leaves the region of interest. This triangle corresponds to particles that will hit the central scatterer. By inspection of Fig. 10 we have

$$l_2' = \frac{(l_1 + l_2)}{2} , \qquad l_1 = \frac{L l_2}{(2 l_2 \cos\alpha + L)} . \tag{C7}$$

Thus

$$\frac{(l_2' - l_2)}{l_2} \approx \frac{\tau_0}{l_2}\frac{dl_2}{dt} = -\frac{l_2 \cos\alpha}{(2 l_2 \cos\alpha + L)} , \tag{C8}$$

where we have introduced the time as $t = \tau_0 n$, $\tau_0 = \sqrt{2}/2$ being a characteristic time between two successive hits against the sides.

Integrating (C8) we obtain

$$\frac{(t - t_0)}{\tau_0} = \frac{L}{\cos\alpha}\left(\frac{1}{l_2(t)} - \frac{1}{l_2(0)}\right) - 2\ln\frac{l_2(t)}{l_2(0)} . \tag{C9}$$

For long t, this means

$$l_2 \approx \frac{L\tau_0}{\cos\alpha}\frac{1}{t} . \tag{C10}$$

Therefore the area is

$$\begin{aligned} A(t) &= 2 l_2(t) L \sin\alpha \\ &\approx 2\tau_0 L^2 \tan(\alpha)\frac{1}{t} \\ &\approx \sqrt{2}\tan(\alpha)\left(1 - \frac{R}{R_c}\right)^2 \frac{1}{t} , \end{aligned} \tag{C11}$$

where we have employed (C5).

In order to evaluate $\tan\alpha$ we calculate the first derivative of (C4) in I' so

$$\tan\alpha = \frac{1}{\sqrt{2}(1 - R/2R_c)} . \tag{C12}$$

Thus we finally obtain

$$A(t) = \frac{(1 - R/R_c)^2}{(1 - R/2R_c)}\frac{1}{t} , \tag{C13}$$

and since

$$g(t) \sim -\frac{dA}{dt}, \qquad t \to \infty \tag{C14}$$

for long time we will have

$$\begin{aligned} g(t) &\sim \frac{(1 - R/R_c)^2}{(1 - R/2R_c)}\frac{1}{t^2} \\ &\sim (1 - R/R_c)^{3/2}\frac{1}{t^2} . \end{aligned} \tag{C15}$$

[1] W. Bauer and G. F. Bertsh, Phys. Rev. Lett. **65**, 2213 (1990).

[2] O. Legrand and D. Sornette, Phys. Rev. Lett. **66**, 2172 (1991); W. Bauer and G. F. Bertsh, *ibid.* **66**, 2173 (1991).

[3] C. F. Hillermeier, R. Blümel, and U. Smilansky, Phys. Rev. A **45**, 3486 (1992).

[4] M. V. Berry, in *Topics in Nonlinear Dynamics (La Jolla Institute)*, Proceedings of the Workshop on Topics in Nonlinear Dynamics, edited by S. Jorna, AIP Conf. Proc. No. 46 (AIP, New York, 1978), p. 16.

[5] Ya. G. Sinai, Russ. Math. Surv. **25**, 137 (1970).

[6] M. V. Berry, Eur. J. Phys. **2**, 91 (1981).

[7] J. D. Meiss, Chaos **2**, 267 (1992).

[8] T. S. Gradshteyn and J. M. Ryzhik, *Table of Integrals, Series and Products* (Academic, New York, 1980).

[9] A. Zacherl, T. Geisel, J. Nierwetberg, and G. Radons, Phys. Lett. **114A**, 317 (1986).

[10] J. P. Bouchaud and P. Le Doussal, J. Stat. Phys. **41**, 225 (1985).

[11] B. Friedman and R. F. Martin, Jr., Phys. Lett. **105A**, 23 (1984).

[12] J. P. Bouchaud and P. Le Doussal, Physica D **20**, 335 (1986).

[13] A. S. Pikovsky, J. Phys. A **25**, L477 (1992).

[14] A. J. Fendrik and M. J. Sánchez (unpublished).